W-Cu composites reinforced by copper coated graphene prepared using infiltration sintering and spark plasma sintering: A comparative study

K. Zhou[a], W.G. Chen[a,*], J.J. Wang[a], G.J. Yan[a], Y.Q. Fu[b,*]

[a] School of Materials Science and Engineering, Xi'an University of Technology, Xi'an, Shaanxi, 710048, PR China
[b] Faculty of Engineering and Environment, Northumbria University, Newcastle upon Tyne, NE1 8ST, UK

ABSTRACT

In order to solve problems of significant interfacial reactions and agglomeration in graphene reinforced W−Cu composites, powders of copper coated graphene (Cu@Gr) were pre-mechanically mixed with tungsten and copper powders, and then graphene doped W−Cu composites were sintered using two different methods, e.g., spark plasma sintering (SPS) and infiltration sintering. Microstructural analysis showed that the doped Cu@Gr powder can effectively inhibit the interfacial reaction between graphene and tungsten, prevent the segregation of graphene, and evenly distribute the copper in the binder phase. When the mixed concentration of Cu@Gr was 0.45 wt%, uniform distributions of W phase and Cu phase were obtained in the composite, and the mechanical properties and conductivity of this composite achieved their best results. When the doping content was further increased to 0.8%, WC phase was found in all alloys, thus resulting in poor mechanical and physical properties. Comparing the microstructures produced using these two methods, the composites prepared using the infiltration sintering method showed network distribution of copper phase and segregation of copper, whereas the composites prepared using the SPS method showed network skeleton phase of tungsten. Although the SPS process was performed in a much shorter time, the mechanical properties of the composites sintered using the SPS process did not show much differences with those sintered using the infiltration sintering method.

1. Introduction

W−Cu pseudo-alloys have superior properties of good electrical and mechanical properties, high resistance to fusion welding and resistance to arc ablation [1–4], therefore, they are widely used as high-voltage contact material, electrode material [5,6] and heat sink material [7]. However, as the working conditions become more and more severe, the mechanical properties and electrical properties of the tungsten-copper composites need to be improved significantly. A third component has often been chosen to add into the W−Cu alloys [8–11] or a new surface treatment technology [1,12] has often been applied to improve their properties. However, these methods do not often show significant improvement of mechanical and electrical properties of the Cu−W alloys for electrical contacts applications.

Graphene, a 2D sp2-orbital carbon sheet, has excellent conductivity, thermal conductivity and mechanical properties [13–16], and is now widely used as a reinforcing phase in alloys. For example, Dong et al. [4] added graphene into tungsten-copper alloy to improve structural uniformity and arc erosion resistance; Wang et al. [17] deposited graphene directly onto the surface of copper nanoparticles to form copper graphene composites, which greatly improved the hardness and anti-friction properties of the nanocomposites.

Due to the extremely large specific surface area ($2630 m^2/g$) [18] of graphene, it is quite common that graphene becomes agglomerated within the composite, which causes the problems of interfacial reactions in the matrix material [19]. This problem can be solved partially by using an electroless plating method to coat a layer of metal particles on the graphene surfaces. For example, Hao et al. [20] used a chemical plating method to deposit silver particles onto the surface layer of graphene, and prepared a silver-based bulk material by doping with 0.5 wt% graphene to obtain a bulk material with uniform microstructure, fine particles and good performance. Mu et al. [21] used a chemical reduction method to obtain a sheet structure of graphene doped with nickel, which was then added into a titanium-based material. The composites effectively solved the problems of poor graphene dispersion and improved the interfacial compatibility between graphene and matrix, therefore greatly improved the strength of titanium-based materials. Wang et al. [22] fabricated copper nanoparticles-modified graphene (Cu-NPs@GN)-reinforced Al matrix composites, which showed an increase in tensile strength and a total elongation of

* Corresponding authors.
  E-mail addresses: wgchen001@263.net (W.G. Chen), richard.fu@northumbria.ac.uk (Y.Q. Fu).

17.5%. They attributed these improvements to the pinning effect of Al_2Cu at the interface, which promotes the load transfer efficiency.

Infiltration sintering is the main preparation technology of tungsten-copper composites. Zhang et al. [23] and Xiong et al. [24] prepared tungsten-copper alloys with different tungsten particle sizes using the infiltration sintering method. Chen et al. [25] prepared a tungsten-copper composite with copper-coated tungsten powders using an infiltration sintering method, and obtained a tungsten-copper material with a uniform network distribution. The discharge plasma sintering technology has also been widely used in recent years with its advantages of lower energy required, shortened sintering time, increased heating rate, and higher density of the sintered material. For example, Ahaubey et al. [26] used a discharge plasma sintering technique to prepare seven layers of W−Cu functionally graded materials. Each layer achieved a high density and good interfaces were formed between different layers. Nachiketa et al. [27] employed spark plasma sintering (SPS) to prepare a silver-based electrical contact material doped with WC without any cracks.

In this paper, graphene reinforced W−Cu composites with different doped graphene contents were prepared using two different methods, i.e., infiltration sintering and SPS. The differences of microstructures, phase distributions and mechanical and physical properties of the composites prepared by these two methods were compared.

2. Experimental method

The raw materials used in this paper are tungsten powder (99.9%, the average particle size of 5–7 μm, obtained from Zhuzhou Cemented Carbide Group Co., Ltd., China) and copper powder (99.999%, the average particle size of 4–5 μm, obtained from Chinese Metallurgical Research Institute, China). The copper-coated graphene composite powders were prepared in-house and the preparation method can be found in our previous paper [28].

The sintering processes of copper-coated graphene reinforced W−Cu composites by the conventional infiltration method and spark plasma sintering are shown in Fig. 1. For the infiltration sintering method, copper-coated graphene powder, copper powder and tungsten powder were mixed according to the ratios listed in Table 1, and then ball milled at a speed of 350 r/min for 4 h with the ball-to-material ratio of 5: 1. The milled powders were then compacted into cylinders (with a diameter of 11 mm and a length of 4 mm) under a pressure of 600 MPa, which makes the compact with a density of 85%. The added amounts of graphene were 0.0 wt%, 0.1 wt%, 0.45 wt% and 0.8 wt%, respectively. The copper block to be infiltrated was placed at the upper end of the compact and sintered in a furnace under the protective Ar atmosphere.
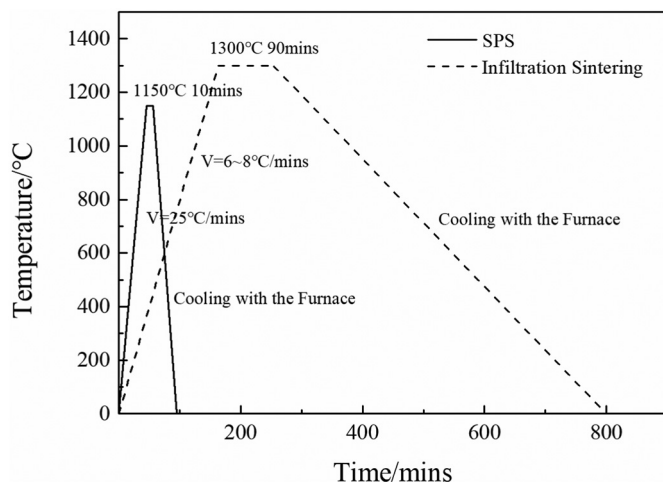
Table 1
Mixing ratios of raw powder materials (in wt%) by different sintering methods.

Sintering method	Alloy composition	Tungsten powder	Copper powder	Cu@Gr	Infiltrated copper block
Spark Plasma Sintering	CuW80	80%	20%	0.0%	–
	CuW80	80%	20%	0.1%	–
	CuW80	80%	20%	0.45%	–
	CuW80	80%	20%	0.8%	–
Infiltration sintering	CuW80	80%	5%	0.0%	15%
	CuW80	80%	5%	0.1%	15%
	CuW80	80%	5%	0.45%	15%
	CuW80	80%	5%	0.8%	15%

The heating rate was 6–8 °C/min, and the sintering temperature was 1300 °C. The sintered block was naturally cooled down to room temperature within the furnace.

For the SPS process, the above-mentioned mixed powder was filled in a graphite mould with a diameter of 15 mm for preloading, and cold pressed with a pressure of 30 MPa. The amount of added graphene were 0.0 wt%, 0.1 wt%, 0.45 wt% and 0.8 wt%, respectively. The pre-fabricated green body in the graphite mould were sintered at a temperature of 1150 °C for 10 min in the SPS sintering chamber protected by argon atmosphere, with a heating rate of 25 °C/min and a pressure of 30 MPa.

The phase distribution of polished W−Cu composites was observed using an inverted metallographic microscope (GX71, OLYMPUS, Japan). An X-ray diffractometer (XRD-7000, Shimadzu, Japan) with Cu Kα radiation at 40 kV and 40 mA was used to analyze the crystalline structures of Cu@Gr W−Cu composites. The scanning speed was 2°/min and the scanning range of 2θ was 10–90° with a step size of 0.02°. Surface morphology of Cu@Gr W−Cu composites was observed using a scanning electron microscope (SEM, TESCAN VEGA3 XMU, TESCAN, Czech Republic) and chemical element analysis was performed using an energy dispersive X-ray spectrometer (EDS, TESCAN, Czech Republic). Detailed morphological characteristics of Cu@Gr W−Cu composites were obtained using a transmission electron microscope (TEM, JEM-3010, JEOL, Japan). Densities of the sintered samples were measured using the Archimedes' water immersion method. The conductivity was measured using a D60K digital metal conductivity meter (Xiamen XinBoTe technology co., Ltd). Samples were sectioned and polished for Vickers micro-hardness measurements, which were performed by applying a 500 g load for 10 s. Four measurements of the micro-hardness were taken at random locations throughout the sample, and the average reading was obtained. The differences in their mechanical properties of the composites were discussed based on their differences in the microstructures.

3. Results and analysis

Fig. 2 shows metallographic structures of Cu@Gr/W-Cu composites sintered using the infiltration method with different doping contents. The gray area is tungsten particles and the light black area is copper phase. The W−Cu composite is a pseudo alloy, so it does not exhibit any second phases in the composite during sintering [29]. Based on the phase diagram of the W−Cu pseudo alloy shown in Fig. 2, the copper phase has changed to liquid at a lower temperature (1084 °C). During the vacuum infiltration sintering, the liquid copper penetrates into the pre-compacted matrix under the combined effects of high temperature diffusion, gravity and capillary effects. Fig. 3(a) shows that for the W−Cu composites without doping with Cu@Gr, the copper molten areas are much larger, and phase agglomeration is more apparent, compared with those for the Cu@Gr doped composites. From Fig. 3, when the doping amount of copper-coated graphene is less than 0.8 wt%, the tungsten and copper phases are distributed quite uniformly, and there is no apparent agglomeration phenomenon. The optimum doping content of copper-coated graphene for the W−Cu composites in this
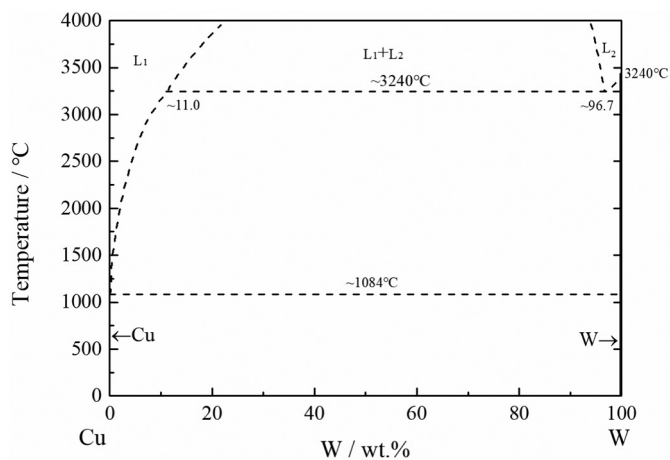

Fig. 1. Curves of sintering process curves of copper-coated graphene reinforced tungsten-copper composites.

Fig. 2. Cu−W binary phase diagram.

study is ~0.45 wt%, showing a uniform microstructure and a network distribution of the copper phase. However, with an increase in the doping amount above 0.8 wt%, the copper phase distribution becomes non-uniform, and there are large voids and apparent segregation in the W−Cu alloy. This is mainly because with a large amount of powders of copper-coated graphene, their dispersion in the composites becomes difficult and non-uniform. This makes excessive copper easily gathered together to form many local "melting spots", thus resulting in copper segregation during the subsequent furnace cooling process.

Fig. 4 shows the metallographic structures of Cu@Gr/WCu composites prepared using the SPS with different doping contents of Cu@Gr. The images show that there are grayish granular substances on the light black substrate. Among them, the gray area is tungsten particles, and the light black area is copper phase. Copper is evenly

distributed around tungsten particles without apparent segregation. From the microstructure of W−Cu composites shown in Fig. 4a, it can be seen that the tungsten and copper phases are uniformly distributed. It can also be observed that some copper areas have irregular polygon shapes, which is a phenomenon of copper enrichment. This phenomenon may be caused by non-uniform heating of copper during sintering, which results in an instantaneous melting of copper in some small areas. The liquid copper leads to an excessive erosion of tungsten skeleton, leaving the polygonal areas within the sintered body.

With the addition of a small amount of copper-coated graphene of 0.1 wt%, the uniform distribution of copper in tungsten-copper alloy is improved but copper is still enriched in some areas as can be observed in Fig. 4b. When the doping content of copper-coated graphene is increased to 0.45 wt%, the tungsten phases are encapsulated by copper phases, which are formed continually and uniformly along the boundary of tungsten particles. It can be observed that the tungsten particles are distributed uniformly whereas the infiltrated copper phases are distributed dispersively, without any significant enrichment area of copper phase. When the doping amount of copper-coated graphene reaches 0.8 wt%, the uniform distribution of tungsten particles can still be observed, however, the dispersion of copper phase is not as uniformly as that of the composites with 0.45 wt% copper-coated graphene (Fig. 4c) and the size of tungsten particles is smaller.

Compared with the tungsten-copper alloy (Fig. 4a) coated with graphene without doping with copper, the tungsten-copper alloy (Fig. 4c) coated with 0.45 wt% copper doped with graphene has more uniform distributions of both tungsten and copper phases. This is because during the SPS process, a fast, efficient and uniformly distributed heating source causes rapid flow of the material, and the molten copper liquid fills the voids in the tungsten skeleton at a high speed. At the same time, the pressure applied at both ends of the holder can enhance the liquid flow of copper in the tungsten-copper alloy, so that the copper phase is uniformly distributed in the tungsten skeleton. The
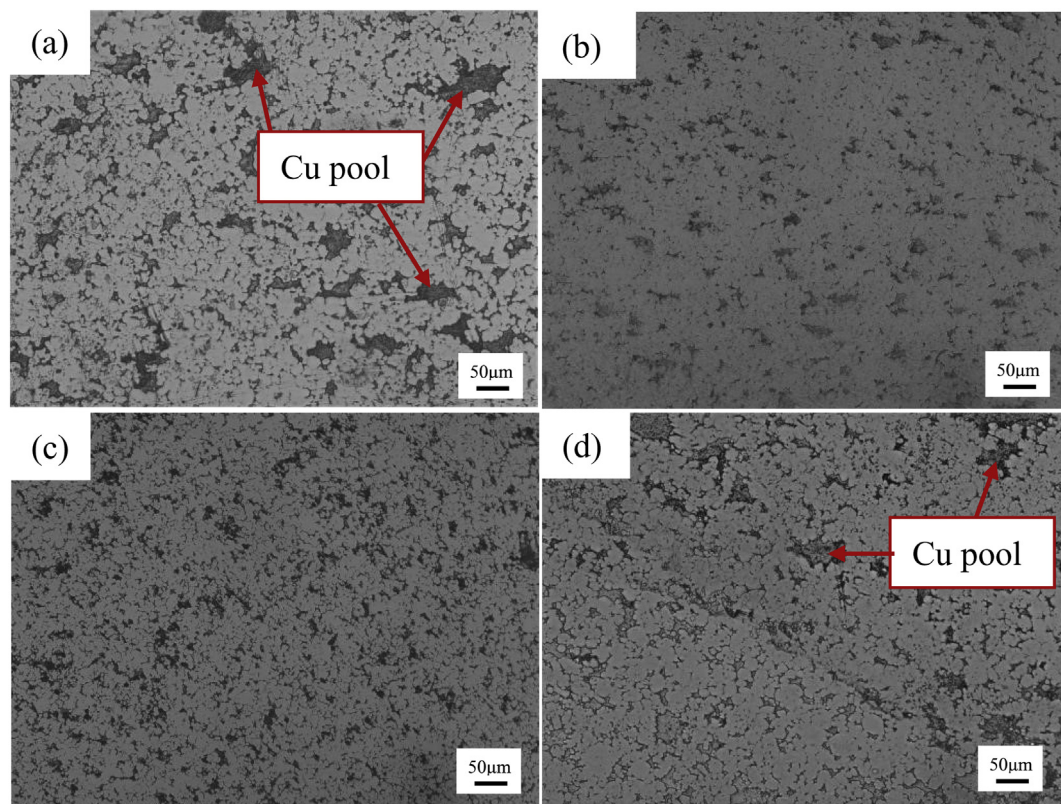

Fig. 3. Optical microscopic images of Cu@Gr/WCu composites by infiltration sintering technology (a) WCu; (b) WCu-0.1% Cu@Gr; (c) WCu-0.45% Cu@Gr; (d) WCu-0.8% Cu@Gr.
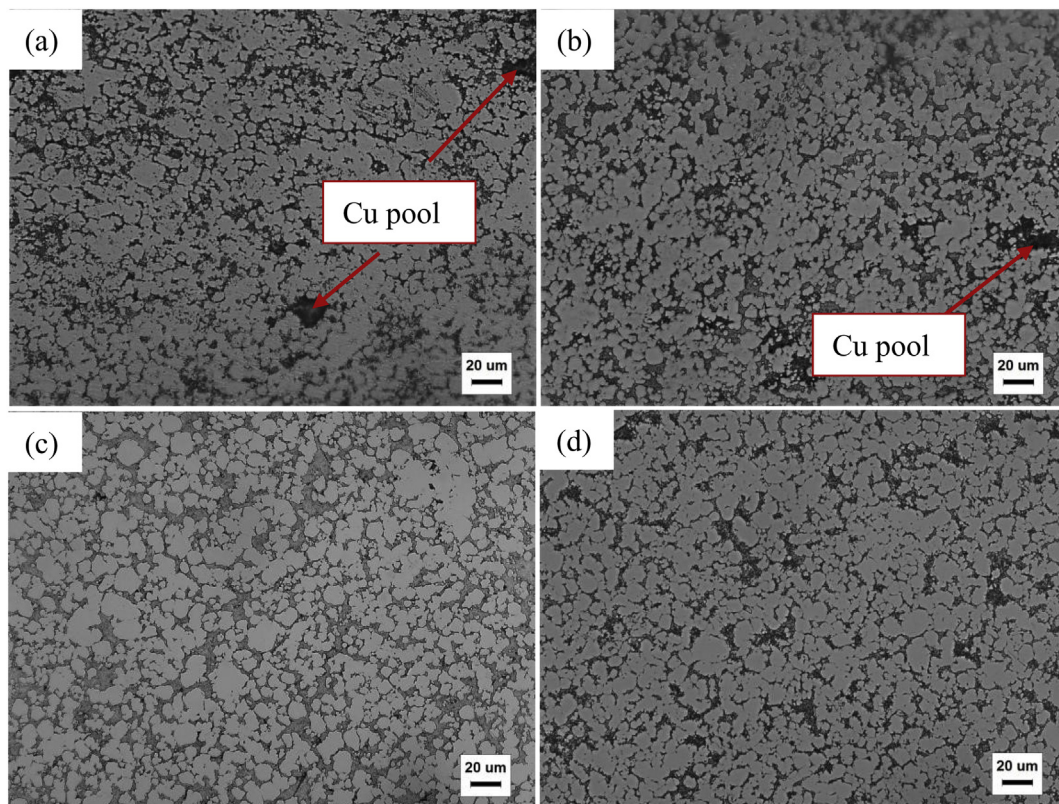
Fig. 4. Optical microscopic images of Cu@Gr/WCu composites by SPS at 1150 °C for 10 min (a) WCu; (b) WCu-0.1% Cu@Gr; (c) WCu-0.45% Cu@Gr; (d) WCu-0.8% Cu@Gr.

plastic deformation can increase the densification degree of the material, which helps to strengthen the densification of the tungsten-copper composite and enhance the interfacial bonding between tungsten and copper. Due to the short sintering time, the significant particle growth which occurs in the long-term sintering of the conventional infiltration sintering can be avoided. Therefore, although the content of graphene is further increased, there is no obvious agglomeration phenomenon observed in the SPS processed samples.

Fig. 5 shows XRD diagrams of tungsten-copper composites doped with different contents of copper-coated graphene prepared using both infiltration sintering and SPS methods. Four crystal planes of (110), (200), (211), (220) corresponding to tungsten appear at 40.264°, 58.274°, 73.175° and 87.169° for copper-doped graphene coated

tungsten-copper alloys sintered using the infiltration method. The (111) and (200) crystal planes of copper are located at 43.316° and 50.448°, respectively. When the doping amounts of copper-coated graphene are 0.45 wt% and 0.8 wt%, the carbon diffraction peaks appear at 26.1°, which is a new phase formed after the copper-coated graphene was added. However, when the doping amount of Cu coated graphene is 0.1 wt%, there is no diffraction peak of carbon because the doping amount of graphene is insignificant. At the same time, when the doping amount of copper-coated graphene is 0.8 wt%, there are three low-intensity peaks at 2θ = 31.511°, 35.641° and 48.296°, which correspond to (001), (100) and (101) facets of WC, respectively.

The tungsten-copper alloys doped with Cu@Gr using the SPS have the similar phases as those obtained from the infiltration sintering.
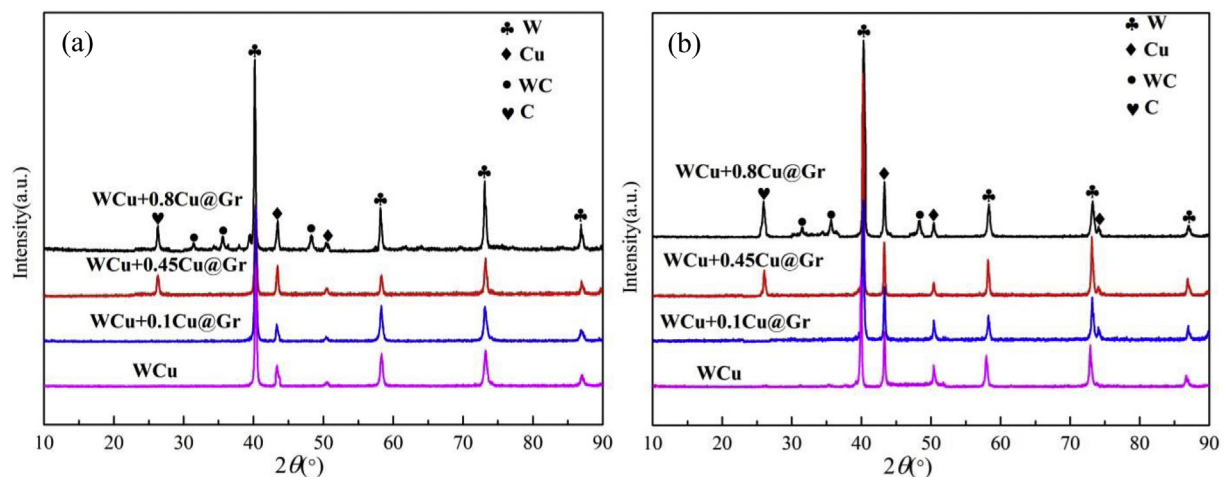

Fig. 5. XRD patterns of WCu composites doped with different Cu@Gr amount of 0.0%,0.1 wt%,0.45 wt% and 0.8 wt% (a)Infiltration sintering technology; (b) SPS.
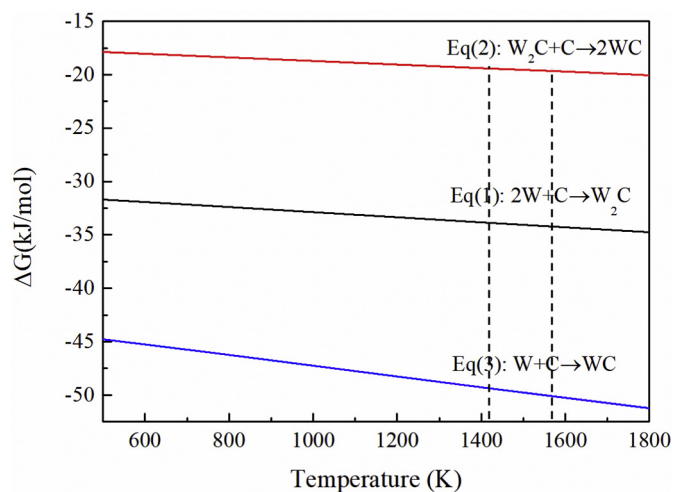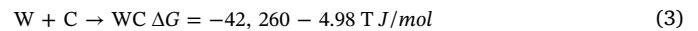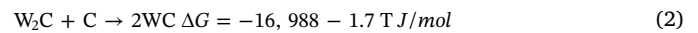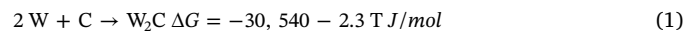
Fig. 6. Ellingham diagram of reaction between tungsten and carbon.

Carbon atoms in graphene will be diffused on the surface of tungsten skeleton at a high temperature. Carbon atoms can easily diffuse into the octahedral gaps of tungsten atoms (the diameter of carbon atoms is 0.154 nm, and the diameter of tungsten atoms is 0.274 nm). The chemical reactions between W and C and their Gibbs free energy values can be expressed as follows:

$$2\,W + C \rightarrow W_2C \; \Delta G = -30,\,540 - 2.3\,T\,J/mol \tag{1}$$

$$W_2C + C \rightarrow 2WC \; \Delta G = -16,\,988 - 1.7\,T\,J/mol \tag{2}$$

$$W + C \rightarrow WC \; \Delta G = -42,\,260 - 4.98\,T\,J/mol \tag{3}$$

From the Eqs. (1)–(3), the Ellingham diagram can be obtained and is shown in Fig. 6. The W−C phase diagram [30] shows that the Gibbs free energy values of Eqs. (1)–(3) are negative in the range of 773 K to 1773 K, so the thermodynamic conditions of these three reactions are satisfied. In the temperature range between 1423 K to 1573 K, the Gibbs free energy of reaction 3 is the lowest and its reaction is the most preferred in theory. However, the reaction between W and C is actually the process in which C atoms gradually diffuse to W, thus increasing the number of C atoms around W atoms. Therefore the detrimental phase W_2C is easily formed in the SPS process. With an increase in the SPS holding time, the activity and concentration of carbon atoms will increase, and the W_2C in the product will be more easily converted into the stable WC phase.

XRD spectra of Cu@Gr/W-Cu composites show that most of the copper coated graphene are not involved in the reactions. It shows that
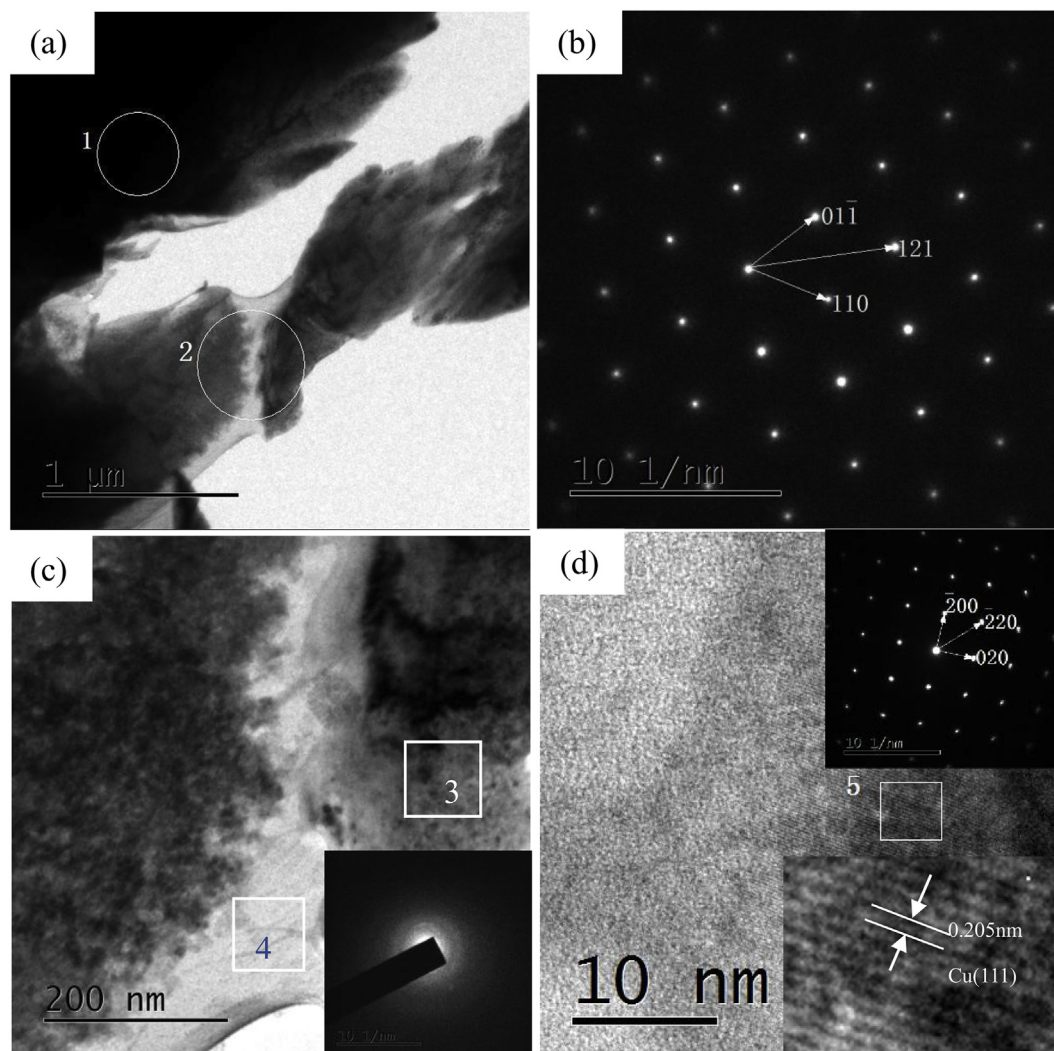

Fig. 7. TEM images of Cu@Gr/WCu composites doped with 0.1 wt% Cu@Gr after infiltration sintering. (a) 0.1wt%Cu@Gr/WCu composites; (b) Electron diffraction pattern of position 1 in Fig. 7(a); (c) High.magnification of position 2 in Fig. 7(a) and an electron diffraction pattern of position 4; (d)The HRTEM image and electron diffraction pattern of position 3 in Fig. 7(c), High amplification of position 5 in Fig. 7(d).
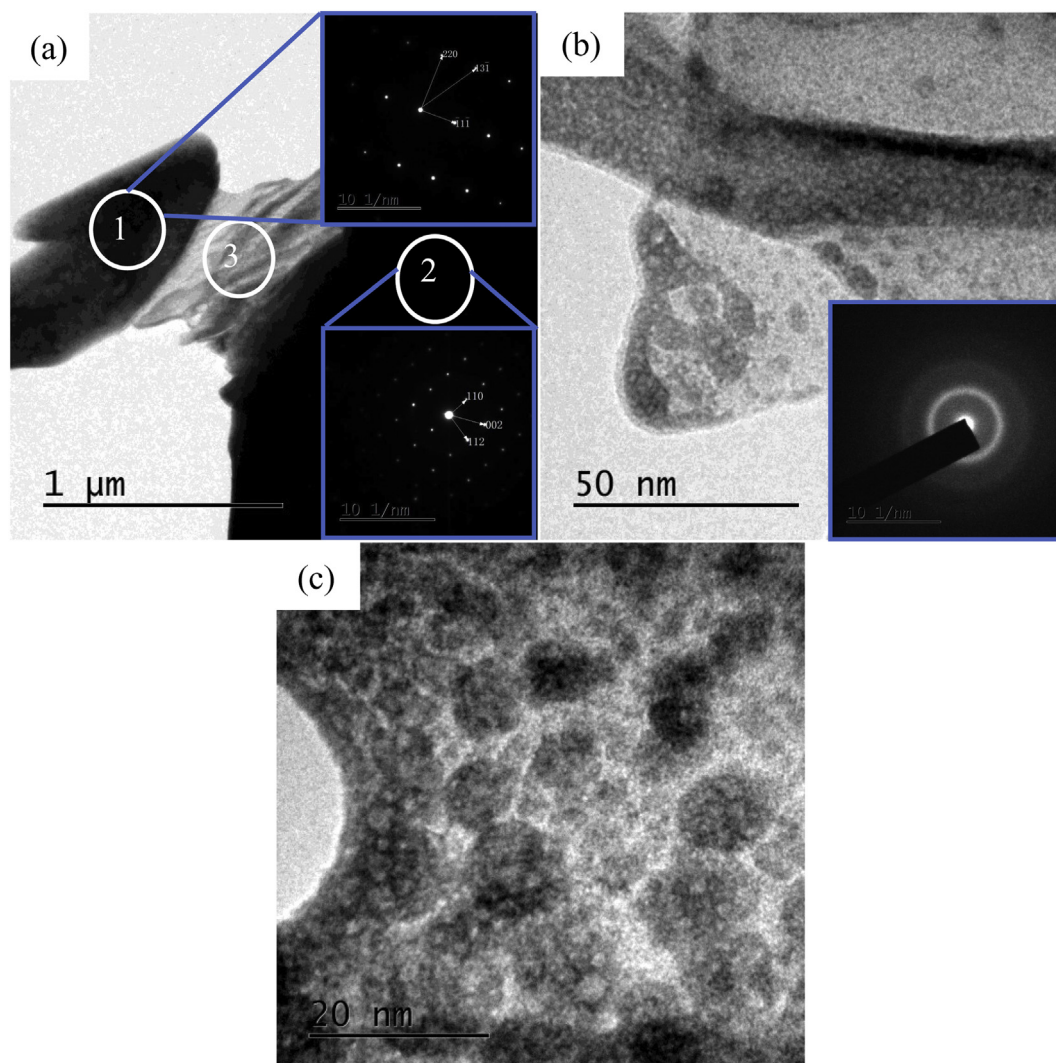
Fig. 8. TEM images of Cu@Gr/W-Cu composites doped with 0.8 wt% Cu@Gr after infiltration sintering. (a) 0.8wt%Cu@Gr/WCu composites and embedded in an electron diffraction pattern positions 1 and 2; (b) High magnification of position 3 in Fig. 8(a), inset is electron diffraction of position 3; (c) High amplification of Fig. 8(b)

the graphene coated with copper can be retained completely, and the graphene in the copper coated graphene can improve the mechanical and electrical properties of W−Cu composites. The particles closely bound to graphene can prevent the direct contact between graphene and tungsten particles, and hence the chemical reaction between graphene and tungsten particles can be prevented. It can be concluded that the copper particles adhered to the graphene surface can prevent the chemical reaction between graphene and tungsten through surface protection. If the surface of graphene is not covered with copper and graphene is directly contacted with tungsten particles, a large amount of tungsten carbide may be produced through chemical reactions between graphene and tungsten skeleton at a high temperature.

Fig. 7a is a low magnification TEM image of W−Cu alloy reinforced by 0.1 wt% copper coated graphene obtained using the infiltration sintering process. For the position 1 in Fig. 7a, the pattern of electron diffraction (Fig. 7b) shows that the black area is tungsten phase. Figs. 7c shows an enlarged TEM image of position 2 in Fig. 7a, revealing the distribution of gray to black and white structures. The electron diffraction pattern of the white region at position 4 in Fig. 7c presents a halo of amorphous structure, which indicates that the white region may be graphene. Fig. 7d shows a high resolution TEM image and electron diffraction pattern of the gray-black region of position 3. As shown in the embedded high-resolution image of position 5 in Fig. 7d, the lattice

fringe spacing is 0.205 nm, which corresponds to the copper (111) crystal plane. This indicates that the gray-black region is copper phase. TEM analysis of copper-coated and graphene-doped W−Cu composites prepared by the infiltration method shows that the sintered W−Cu composites are mainly composed of tungsten phase, copper phase and graphene. After sintering, tungsten phase and graphene have not chemically reacted to form WC. The microstructure of copper-coated graphene has not been destroyed during the sintering, which could play an important role in strengthening the W−Cu matrix composites.

Fig. 8 is a TEM image of 0.8 wt% copper coated graphene reinforced tungsten-copper alloy prepared using the infiltration sintering method. The electron diffraction pattern shown at the upper right corner embedded in Fig. 8a indicates that the position 1 in Fig. 8a is copper phase. Electron diffraction pattern of position 2 in the lower right corner of Fig. 8a shows that it is a tungsten phase. Fig. 8b shows an enlarged view of the gray area in position 3 in Fig. 8a, Fig. 8c is a high-magnification TEM image of that shown in Fig. 8b. It can be seen that the gray-black granular phase is distributed uniformly in a gray background of uniform substrate. From the electron diffraction pattern shown in the inset of Fig. 8b, this gray-black granular phase is graphene. Results indicate that when the doping amount of copper coated graphene is increased up to 0.8 wt%, the copper coated graphene could prevent the direct reaction of graphene and tungsten to form tungsten carbide, and graphene can
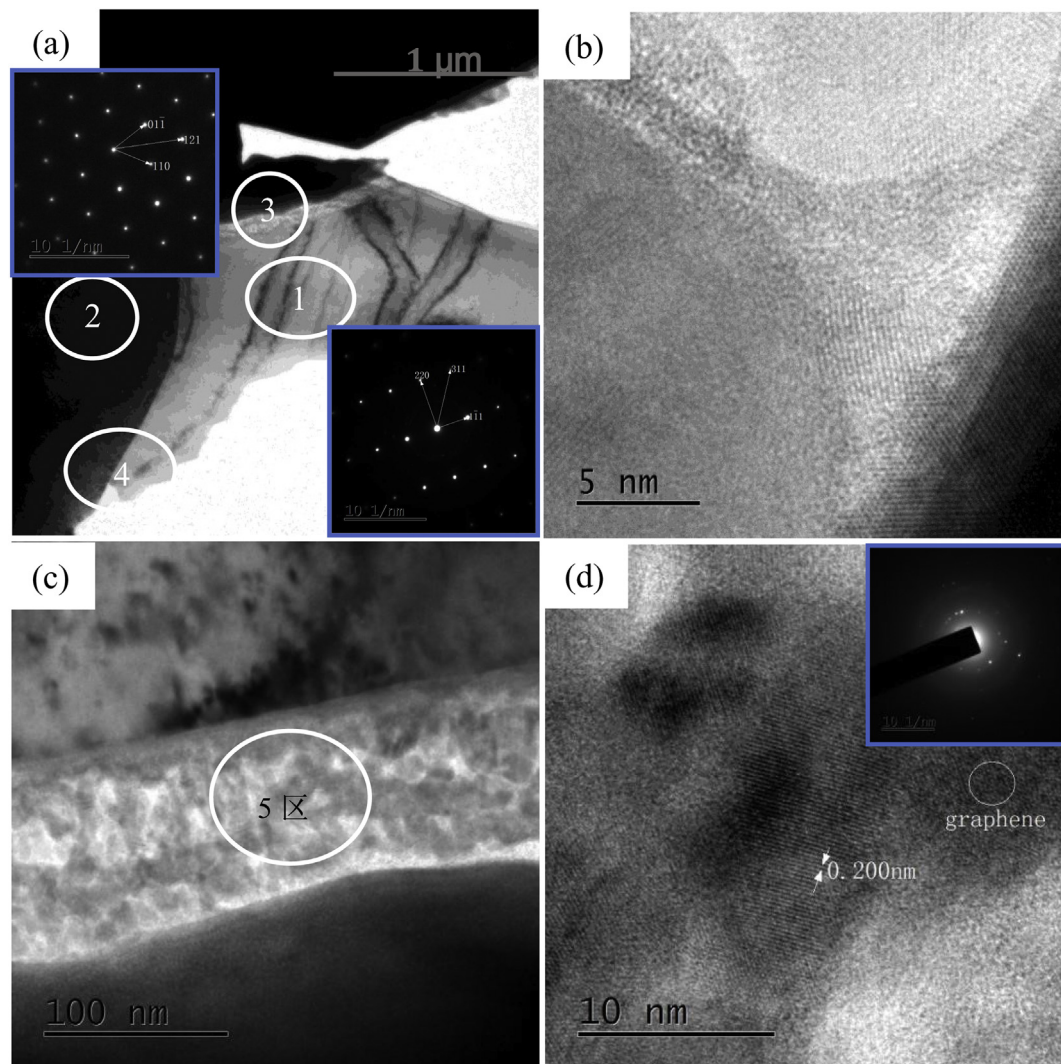
Fig. 9. TEM images of Cu@Gr/WCu composites doped with 0.8 wt% Cu@Gr after SPS. (a) 0.8 wt% Cu@Gr/WCu composites, Electron diffraction pattern and calibration of positions 1 and 2 in Fig. 9(a); (b) High magnification of marked position 4 in Fig. 9(a); (c) High magnification of position 3 in Fig. 9(a); (d) The HRTEM image and Electron diffraction pattern of position 5 in Fig. 9(c);

Table 2
The density, electrical conductivity and hardness of W80Cu20 composites by infiltration sintering and spark plasma sintering containing 0.0 wt%, 0.1 wt%, 0.45 wt% and 0.8 wt% Cu@Gr, respectively.

Sintering method	Doping amount (wt %)	Measured density (g/cm^3)	Electrical conductivity(% IACS)	Hardness (HV)
Infiltration Sintering	0.0%	15.1	35.8	226
	0.1%	15.1	38.6	231
	0.45%	14.9	46.7	238
	0.8%	14.7	36.8	264
Spark Plasma Sintering	0.0%	15.1	24	207
	0.1%	15.1	38.6	227
	0.45%	15.0	43.3	238
	0.8%	14.8	31.2	254

still maintain its original structure.

Fig. 9 shows a TEM image of tungsten-copper alloy doped with 0.8 wt% copper coated graphene sintered using SPS method. From the electron diffraction pattern of gray area of position 1 in Fig. 9a, we can identify that the black area 2 is copper and the black area is tungsten. Fig. 9b is an enlarged image of position 4 in Fig. 9a. It can be seen from this figure that the structure is a combined copper and tungsten phases.

Fig. 9c is an enlarged TEM image of the gray-white area in Fig. 9a, and Fig. 9d is the corresponding HR-TEM image, as well as electronic diffraction patterns (the embedded image). It can be seen from the TEM image that the gray granular microstructures are uniformly distributed within the white ones. The lattice fringe spacing of the HR-TEM image shown in Fig. 9d was calculated and it is ~0.200 nm, corresponding to the plane spacing of the {111} crystal family of copper. From the amorphous halo ring of the electron diffraction pattern, it can be concluded that the white substrate in Fig. 9c is graphene. From the microstructural analysis, we can conclude that graphene and copper are well distributed, and tungsten carbide phase has not been detected.

Comparisons of the above images reveal that the gap of tungsten particles is much larger after the infiltration sintering, and the volume of copper phase between W−W grain boundaries is larger, which reduces the good connectivity of W−W grain boundaries. A possible network distribution of bonded phase copper is formed. However, due to the combined actions of both large compressive stress and short-time sintering in the process of SPS, the infiltration of copper phase into the W−W grain boundary was reduced. The connectivity of W−W grain boundary was improved, and the tungsten grain was relatively small. Therefore, the SPS processed composites shows a better network of tungsten phases with the copper phase uniformly distributed inside.

Table 2 lists the measured results of density, electrical conductivity

and hardness of W−Cu composites prepared using two types of sintering methods. The electrical conductivity values of all these composites are firstly decreased but then increased with the gradual increase of the content of Cu@Gr. The hardness values are continuously increased with the increase of the content of Cu@Gr.

For the infiltration sintered composites, when the amount of the copper-coated graphene is increased to 0.45 wt%, the hardness of the tungsten-copper alloy is 238 HV, and the electrical conductivity is 46.6% IACS., which are increased by 5% and 30.2% compared to those of the WCu alloy without adding copper-coated graphene. However, when the doping amount is further increased up to 0.8 wt%, the copper-coated graphene are difficult to be dispersed in the tungsten-copper matrix. Simultaneously the graphene becomes distributed in the grain boundary (see Fig. 3), and thus influences the mean free path of the conducting electrons. Therefore, the conductivity of the tungsten-copper alloy becomes decreased. It can be seen from the XRD result shown in Fig. 5 that excess graphene will react with tungsten to form tungsten carbide, which increases electron scattering and hinders the infiltration process and increases the porosity. This increased porosity will significantly reduce the electrical conductivity and the density of the tungsten-copper alloy [8].

For the composites prepared using the SPS, the hardness values increase with the added contents of the copper-coated graphene. As a reinforcing phase, graphene can act as a barrier for the free movement of dislocations, thus improving the strength of the material. As the content of graphene is increased, this pinning effect to the dislocations is continuously enhanced, so that the hardness of the tungsten-copper alloy are continuously improved. When the doping amount is 0.45%, the conductivity of the tungsten-copper composite reaches 43.1% IACS. The density generally decreases with the increase of doping content as listed in Table 2. However, due to the existence of large discharge field and the large pressure applied during the SPS process, which can accelerate the migration of atoms, its density is slightly higher than those obtained using the infiltration sintering method. However, the sintering temperature of SPS is slightly lower, and the time is significantly shorter than that of infiltration sintering, so the properties of composite materials prepared using these two methods do not show significant differences. This is consistent with the previously observed microstructures.

4. Conclusion

In this paper, copper-coated graphene reinforce tungsten-copper composites were prepared using both infiltration sintering and spark plasma sintering, and the microstructures and properties of the composites prepared using these two methods were compared. The following conclusions can be drawn from the present work:

1) The effect of doping amount of copper-coated graphene on the microstructures of tungsten-copper composites was studied. Copper-coated graphene powder can prevent the interfacial reactions between graphene and tungsten, prevent the segregation of graphene, and the copper phases are evenly distributed in the substrate. With an increase in the doping content of copper-coated graphene, the structure distribution of W−Cu alloy becomes more homogeneously. The network distribution of copper phase is formed after the infiltration sintering process. The skeleton of tungsten phase has a network shape, inside which the copper phase is distributed after the SPS process.

2) Density, electrical conductivity and hardness for the composite with the doping of 0.45 wt% using the infiltration sintering have values of 14.9 g/cm^3, 46.7% IACS and 238 HV, respectively. Whereas those values using the spark plasma sintering are 15.0 g/cm^3, 43.3% IACS and 238 HV. However, when the doping content is increased to 0.8%, WC phase appeared in all the composites. There was a small amount of copper segregated inside alloys for the infiltration

sintered samples compared with those obtained from the SPS.

References

[1] W.G. Chen, P. Feng, L.L. Dong, et al., The process of carburization and high temperature wear behavior of infiltrated W-cu composites, Surf. Coat. Technol. 353 (2018) 300–308.

[2] Q. Zhou, P.W. Chen, Characterization of fine-grained W–10wt.% cu composite fabricated by hot-shock consolidation, Int. J. Refract. Met. Hard Mater. 52 (2015) 137–142.

[3] W.G. Chen, M.Z. Chen, L.Q. Xing, et al., Effect of doping electrical arc characteristic WCu electrical contact materials, Chin J Nonferrous Met 19 (11) (2009) 2029–2036.

[4] L.L. Dong, W.G. Chen, N. Deng, et al., Investigation on arc behaviors and mechanism of W70Cu30 electrical contact materials adding graphene, J. Alloys Compd. 696 (2017) 923–930.

[5] X.G. Wang, H.L. Zhang, W.J. Li, et al., Effect of preparation process on microstructure and arc ablation resistance of WCu30 alloy, Rare Metal Mater. Eng. 44 (1) (2015) 140–144.

[6] J.L. Fan, T. Liu, S. Zhu, et al., New processing technology and prospective application of high performance W-cu composites, Cemented Carbide. 28 (1) (2011) 56–65.

[7] L.M. Luo, X.Y. Tan, X.Y. Ding, et al., Fabrication of W/cu graded heat-sink materials by Electroless plating and powder metallurgy, Rare Metal Mater. Eng. 45 (8) (2016) 1983–1987.

[8] X.H. Yang, S.H. Liang, X.H. Wang, et al., Effect of WC and CeO$_2$ on microstructure and properties of W-cu electrical contact material, Int. J. Refract. Met. Hard Mater. 28 (2010) 305–311.

[9] F. Zhuge, Z.Z. Ye, F.Z. Wang, et al., Nanocomposite W-4.5%ThO$_2$ thermionic cathode, Mater. Lett. 57 (2003) 2776–2779.

[10] Z.L. Lu, L.M. Luo, J.B. Chen, et al., Fabrication of W-cu/CeO$_2$ composites with excellent electric conductivity and high strength prepared from copper-coated tungsten and ceria powders, Mater. Sci. Eng. A 626 (2015) 61–66.

[11] L.L. Dong, W.T. Huo, M. Ahangarkani, et al., Microstructural evaluation and mechanical properties of in-situ WC/W-Cu composites fabricated by rGO/W-Cu spark plasma sintering reaction, Mater. Des. 160 (2018) 1196–1207.

[12] H.M. Gao, W.G. Chen, Z.J. Zhang, Evolution mechanism of surface nano-crystallization of tungsten-copper alloy, Mater. Lett. 176 (2016) 181–184.

[13] R.S. Edwards, K.S. Coleman, Graphene synthesis: relationship to applications, Nanoscale 5 (2013) 38–51.

[14] A.A. Balandin, S. Ghosh, W.Z. Bao, Superior thermal conductivity of singer-layer graphene, Nano Lett. 8 (3) (2008) 902–907.

[15] H.C. Schniepp, J.L. Li, M.J. Mcallister, et al., Functionalized single Graphene sheets derived from splitting graphite oxide, J. Phys. Chem. B 110 (17) (2006) 8535–8539.

[16] A. Kumar, K. Sharma, A.R. Dixit, A review of the mechanical and thermal properties of graphene and its hybrid polymer nanocomposites for structural applications, J. Mater. Sci. 54 (8) (2019) 5992–6026.

[17] S.Y. Wang, S.B. Han, G.Q. Xin, et al., High-quality graphene directly grown on cu nanoparticles for cu-graphene nanocomposites, Mater. Des. 139 (2018) 181–187.

[18] M.D. Stoller, S. Park, Y.W. Zhu, et al., Graphene-based Ultracapacitors, Nano Lett. 8 (10) (2008) 3498–3502.

[19] X. Huang, X.Y. Qi, F. Boey, et al., Graphene-based composites, Chem. Soc. Rev. 41 (2) (2012) 666–686.

[20] X. Hao, X.H. Wang, S.M. Zhou, et al., Microstructure and properties of silver matrix composites reinforced with Ag-doped graphene, Mater. Chem. Phys. 215 (2015) 327–331.

[21] X.N. Mu, H.M. Cai, H.M. Zhang, et al., Uniform dispersion and interface analysis of nickel coated graphene nanoflakes/pure titanium matrix composites, Carbon 137 (2018) 146–155.

[22] J. Wang, X. Zhang, N.Q. Zhao, et al., In situ synthesis of copper-modified graphene-reinforced aluminum nanocomposites with balanced strength and ductility, J. Mater. Sci. 54 (7) (2019) 5498–5512.

[23] Q. Zhang, S.H. Liang, B.Q. Hou, et al., The effect of submicron-sized initial tungsten powders on microstructure and properties of infiltrated W-25 wt.% cu alloys, Int. J. Refract. Met. Hard Mater. 59 (2016) 87–92.

[24] X.J. Xiong, Y.X. Liu, Effect of tungsten particle size on structures and properties of infiltrated W-cu compacts for electrodes, Mater. Sci. Eng. Powder Metall. 12 (2) (2007) 101–105.

[25] W.G. Chen, Y.G. Shi, L.L. Dong, et al., Infiltration sintering of WCu alloys from copper-coated tungsten composite powders for superior mechanical properties and

arc-ablation resistance, J. Alloys Compd. 78 (2017) 196–205.

[26] A.K. Chaubey, R. Gupta, R. Kumar, et al., Fabrication and characterization of W-cu functionally graded material by spark plasma sintering process, Fusion Eng Des 135 (2018) 24–30.

[27] N. Ray, B. Kemof, G. Wiehl, et al., Novel processing of Ag -WC electrical contact materials using spark sintering, Mater. Des. 121 (2017) 262–271.

[28] Y.L. Xue, W.G. Chen, J.J. Wang, et al., Formation mechanism and cohesive energy analysis of metal-coated Graphene Nanocomposites using in-situ co-reduction method, Materials 11 (11) (2018).

[29] T.B. Massalski, H. Okamoto, P.R. Subramanian, et al., Binary Alloy Phase Diagrams, 2nd ed, ASM International, USA, 1990.

[30] S.A. Humphry-baker, W.E. Lee, Tungsten carbide is more oxidation resistant than tungsten when processed to full density, Scr. Mater. 116 (2016) 67–70.